Two-zone microstructures in Al-18Si alloy powders

J. E. Spinelli [a,b,*], A-A. Bogno [b], and H. Henein [b]

[a] Department of Materials Engineering, Federal University of São Carlos, São Carlos, SP 13565-905 Brazil.
[b] Department of Chemical and Materials Engineering, University of Alberta, Edmonton, AB T6G 2G6 Canada.

Abstract

Hypereutectic Al-18wt. %Si alloy is widely used in automotive industry as a wear resistant alloy for engine components. However, in the last few years, this traditional composition is being considered for processing by different rapid solidification methods. Positive points include its low thermal expansion and uniform distribution of surface oxides. Nevertheless, microstructural aspects of Al-Si powders of 18 wt. % Si still need to be addressed, such as, the eutectic Si morphology, size and distribution generated by different process conditions during rapid solidification. Based on a detailed quantitative analysis of the microstructures of rapid solidified Al-18wt%Si in this work, solidification conditions that yield specific Si morphologies, Si spacing and thermal cooling conditions are outlined. The focus is determining the solidification conditions that will yield a specified shape of eutectic Si. It is shown that Si morphology is dependent on a combination of growth velocity (based on modified J-H model) and temperature gradient. Furthermore, the highest hardness is achieved with globular morphologies of Si. The processing conditions required to achieve these properties are outlined.

Keywords: Impulse Atomization; Powders; Al-Si; Eutectic growth; Morphology; Microstructure; Hardness.

---

* Corresponding author → E-mail address: spinelli@ufscar.br (J.E. Spinelli)

1. Introduction

Al-Si alloys containing from 4wt.% to 22wt.% Si comprise more than 90% of all Al-based castings. Parts manufactured with these alloys have a wide range of industrial applications due to their excellent castability, crack resistance, good corrosion resistance, good weldability, low density and high strength [1-3]. Hypereutectic Al-Si alloys are widely used and researched in the automotive and aerospace sectors due to their low coefficient of thermal expansion, high temperature resistance, good wear resistance and high strength [3,4]. As an alternative to the conventional hypoeutectic Al-Si, there is growing interest in hypereutectic Al-Si alloys as a candidate material for high-quality engines because a higher volume fraction of silicon would result in superior properties [5,6]. Regarding the increasing applications of these alloys in the automotive and aeronautical industries, the weight factor of Si is directly related to improved energy efficiency of engines [7,8]. By the virtue of their high thermal conductivity and a thermal expansion coefficient (7-9 x 10^{-6} $^{o}C^{-1}$) similar to pure silicon [9], hypereutectic Al-Si alloys show a broad range of commercial applications also in electronic packaging industries.

These characteristics of hypereutectic Al-Si alloys have also aroused interest in the fields of rapid solidification technologies, such as fusion casting technology, powder metallurgy and spray deposition method [10,11]. Again, the low thermal expansion and uniform distribution of oxides on the powder surface are amongst the advantages of these alloys. Understanding the microstructure evolution in these powders and the corresponding processing conditions is critical to developing a knowledgebase for their efficient and effective utilization involving rapid solidification. Determination of solidification conditions might yield a specified shape of Si in hypereutectic Al-Si alloys. This shape is able to tailor the alloy mechanical properties.

Observations by scanning electron microscopy (SEM) and transmission electron microscopy (TEM) of gas-atomized 18 wt.% Si alloy powders indicate a continuous dendritic-cellular-microcellular transition that occurs when particle size is decreased [12]. Even though a range of morphologies was observed, each morphology was associated with a certain range of powder size. In contrast, Boettinger and collaborators

[13] observed the presence of two microstructural zones in single rapidly solidified powders of Al-8wt. %Fe alloy generated by gas-atomization. These authors observed the occurrence of different morphologies emanating from a single nucleation event on the powder surface. The first zone solidifies with a fine cellular interface, followed by a recalescence step proportional to the volume fraction of solid within the cellular structure. Then, a coarser structure forms and grows until the entire powder solidifies. The change in growth velocity produces a strongly time-dependent solidification process and a resulting microstructure, which varies across the powder dimensions.

While lamellar eutectic structure has been observed for large and midrange powder sizes of Al-18wt.%Si [12] generated by gas atomization, a nanocrystalline mixture of Si and Al appears to occur in the case of the smallest powder size ranges. Despite the very high solidification velocities (~110mm/s) of the Al-18Si alloy associated with the very small powders, the morphology of the Si nanocrystals was not elucidated. Hosch *et al.* [14] observed for Al-Si eutectic composition that at low velocities (<250 μm/s), flake is the resulting Si morphology. In contrast, higher velocities result in the activation of additional in-plane growth directions leading to the formation of in-plane rod (fibrous) structures. In rapid solidification processes, such as laser surface remelting (LSR), a globular morphology has been observed for a laser scan speed of 1200 μm/s [15]. Srivastava *et al.* [16] reported that the eutectic microstructure in spray-deposited Al-18Si alloy is significantly modified with formation of globular Si phase of the eutectic constituent. In this case, the growth of eutectic Si globules has not been related to either solidification velocity or cooling rate. Despite suggesting that the eutectic silicon morphology can evolve from globules to fibers, the critical solidification parameters governing the morphologies of this phase under fast cooling conditions have not been determined so far.

As Al-Si system exhibit a skewed couple zone [17,18], a variety of microstructures including cellular/dendritic arrangements and eutectics can be formed during rapid solidification processes. In the case of the Al-Si powders generated by gas-atomization, the coupled zone calculations [19] showed that a eutectic structure would result for a small range of undercooling which generally corresponds to large powders in size [20]. As the undercooling is increased, a microstructural transition from the eutectic to a dendritic array is observed [19,21]. Eutectic undercoolings using Trivedi–Magnin–Kurz (TMK) model were estimated as well as the eutectic spacing (λ) of Al-18wt. % Si powders [12]. Two additional implications regarding the observed morphologies can be considered [12,19]:

i. consideration of nucleation phenomena would affect the overall selection dynamics of Si morphologies;

ii. comparison of predicted morphologies and those observed in the powder microstructures is not always in agreement, especially on the calculated boundaries of the couple zone for undercoolings values higher than the theoretical limit value of 15K for Al -18wt.% Si.

Few studies have focused on correlating the microstructure sizes and morphologies of Al-Si powders of 18 wt. % Si with solidification parameters such as cooling rate, undercooling or growth velocity. Impulse atomization (IA) technique, by the virtue of its capability of producing powders of controlled size and predictable cooling rate, is deemed a suitable method for understanding rapid solidification characteristics [22-24]. Therefore, a systematic study of microstructure evolution of rapidly solidified Al-18Si powders produced by this technique will provide a quantitative knowledge on the morphology, size and hardness related to the solidification parameters.

In the current study, Al-18wt% Si powders of size varying from 75μm to 500μm were generated by IA under helium atmosphere. Firstly, the two distinct microstructure zones within the powders as well as the variation of eutectic microstructural length-scale along the powder diameter will be investigated. Secondly, the analysis of IA powders by mapping out a wide range of eutectic microstructures coupled with two mathematical approaches to determine interface velocity and cooling rate will allow the processing history to be inferred. Finally, the implications of Si morphology and size on microhardness will be considered.

2. Experimental procedure

2.1. Materials and methods

Rapidly solidified Al-18wt. %Si powders of different sizes were generated by IA under helium atmosphere. A quantity of 300g of high purity Al (99.99%) and commercial purity (CP) Si (99.9%) was melted in a dense high purity graphite crucible by induction heating up to 1500ºC in order to melt Al and Si. Then the temperature was brought down to 850°C (~ 190 ˚C above the equilibrium *liquidus* temperature of the alloy) and held for 1 hour before atomization. Detail description of the process is given elsewhere [23-25]. It is worth noting that, prior to melting and atomization, it was ensured that the oxygen level in the atomization chamber was less than 20 ppm. The solidified powders were made to land in an oil filled beaker, then washed, dried and sieved into different size ranges varying from <75 µm to 1000 µm. For this paper, the following ranges of powder sizes (in µm) have been investigated: <75, 90-106, 106-125, 212-250, 300-355 and 425-500. The average size of each range is used for some of the subsequent analysis.

The powders for each size range were separately mounted, polished, etched with Keller's reagent during 10-20s, and then examined using an optical microscope. The overall microstructure of each investigated powder was observed using a motorized BX61 Olympus optical microscope. When mounted in epoxy the powders were deposited at the bottom of the mold. In the epoxy mount, the powders settle and with successive grinding and polishing of the mounted samples, the cross section of the diameter of each powder could be viewed in 2D imaging. This procedure was carried out not only to locate the nucleation site but also to determine the relative fractions occupied by the two distinct microstructure zones. One metallographic sample was prepared of the full size range of powders for visualization purposes as will be described in Fig. 1a.

The length-scale of the eutectic was determined by the Si spacing, λ, measurements using line intercept method [26], for the powders 106-125 µm, 212-250 µm and 425-500 µm in size. Considering that both the scale of the microstructure and the transition in morphologies depend upon solidification conditions, λ was determined as a function of position on the powder cross sections, from the nucleation point to the surface. A total of 6 positions per powder cross section were investigated. The large and elongated primary Si particles formed within the coarse zone of the powder were adopted as reference points indicating preferential growth direction during solidification.

In order to reveal details regarding the morphologies of the eutectic Si, SEM analyzes in both Secondary Electrons (SE) and In-Lens detector modes were carried out on the etched samples. The instrument used was a Zeiss Sigma Field Emission SEM equipped with a Bruker energy dispersive X-ray spectroscopy (EDS). The hardness of the samples was assessed using a Buhler VH 3100 microhardness machine. The device was calibrated using a manufacturer provided steel block. Five indentations were applied on each investigated powder cross section, at the corresponding abovementioned 6 positions, with a load of 50gf for a holding time of 15s.

2.2. Theoretical models

Since the Si spacing was experimentally determined for different powder sizes of the Al-18wt. % Si alloy as well as for various relative distances along the powders, the interface undercoolings and growth rates were determined using the following equations as described by Gunduz [27]:

$$\lambda^2 V = \frac{\phi K_2}{K_1}, \tag{1}$$

$$\lambda \Delta T = \left(\phi^2 + 1\right) K_2, \tag{2}$$

$$K_1 = \frac{\overline{m} C_0^*}{D} \frac{P}{f_\alpha f_\beta}, \tag{3}$$

$$K_2 = 2\overline{m}\left(\frac{\Gamma_\alpha \sin\theta_\alpha}{|m_\alpha| f_\alpha} + \frac{\Gamma_\beta \sin\theta_\beta}{|m_\beta| f_\beta}\right), \tag{4}$$

where m_α and m_β are the *liquidus* slope of the phases, $\overline{m}$ is weighted *liquidus* slope, f_α and f_β are volume fractions of the phases, P is function of the volume fraction as detailed by Gunduz *et al.* [27], c_0^* is weighted eutectic tie-line length, D is diffusion coefficient of Silicon in the liquid, Γ_α and Γ_β are the Gibbs–Thomson coefficients and θ_α and θ_β are contact angles related to the phases forming eutectic.

Considering that the Al-Si is characterized as being an irregular faceted-nonfaceted eutectic, the variation of average eutectic spacing, and eutectic interface undercooling with growth as proposed originally by Jackson and Hunt [28] can be generalized for the irregular eutectic growth by inserting a dimensionless operating parameter ϕ of 2.3 as defined for Al-Si [29]. The other necessary physical properties of the Al-Si eutectic can be found in Table 1.

Table 1. Summary of data used for the investigated Al-Si alloy [12,29,30-33].

Property/Parameter	**Symbol/Unit**	**Values**
Diffusion coefficient of Si in the liquid	D [$m^2.s^{-1}$]	4.3×10^{-9}
Length of eutectic tie-line	C_0^* [wt pct]	98.2
α-phase *liquidus* slope	m_α [K. (wt pct)$^{-1}$]	7.5
β-phase *liquidus* slope	M_β [K. (wt pct)$^{-1}$]	17.5
Gibbs-Thomson coefficient (α-phase)	Γ_α [K.m]	1.96×10^{-7}
Gibbs-Thomson coefficient (β-phase)	Γ_β [K.m]	1.7×10^{-7}
Angle of α phase	$\theta\alpha$ [deg]	30.0
Angle of β phase	$\theta\beta$ [deg]	65.0
Volume fraction (α phase)	f_α [––]	0.873
Volume fraction (β phase)	f_β [––]	0.127
Extremum condition parameter	ϕ [––]	2.3
Latent heat of fusion	L [$J.kg^{-1}$]	397,300
Melt heat capacity	c_p [$J.kg^{-1}.K^{-1}$]	920.0
Density of the liquid	d_L [$Kg.m^{-3}$]	2,650
Thermal conductivity of the liquid	k_L[$W.m^{-1}.K^{-1}$]	70.0

Given that the volume fraction of the fine zone formed from the nucleation site was experimentally determined for different powder sizes of the Al-18wt. % Si alloy, the nucleation undercooling (ΔT_N) could be estimated. In this case, it is considered that at the end of recalescence, the solid volume fraction of the powder, *f*, refers to the fine eutectic zone is $\dfrac{\Delta T_N}{(L^{'}/cp)}$, where L' is the fraction of the latent heat of fusion (L) (corresponding to *f*) and cp is the melt heat capacity.

According to Martin and co-authors [34], during recalescence, cooling rate (CR) is large so solidification is considered as adiabatic. The left hand side term of the well-established equation governing the overall heat balance can be ignored, resulting in:

$$cp\frac{dT}{dt} = L\frac{df}{dt}, \qquad [5]$$

Integrating from f=0 at $T=T_N$:

$$T - T_N = \frac{L}{cp} f \quad or \quad \Delta T_N = f_{fine}.\Delta T_{hyp} \qquad [6]$$

So, ΔT_N can be the estimated by the product of the solid fraction f_{fine} formed during microstructure development in fine zone and the characteristic hypercooling limit of the melt, ΔT_{hyp}, where L is 397,300 J/kg and cp is 920.0 J/(kg.K) for Al-Si [32,33].

3. Results and discussions

3.1. Characterization of microstructure

Three general features of microstructure were observed in the powders: a fine zone composed of the eutectic α-Al+Si, a zone mainly formed by aligned primary Si particles, and a coarse eutectic zone enveloping the aligned Si particles. The occurrence of these microstructures is seen in all examined size ranges, i.e., from 75 μm to 425-500 μm. The fine zone eutectic ("A" in Fig. 1) is a structure which grows from a single nucleation site often occurring near the center of the powder. This microstructure near the point of nucleation is extremely fine. Elongated primary Si particles (Fig. 1c) in the microstructure seem to radiate from the solidified fine eutectic zone, while coarser eutectic envelops the elongated Si particles.

Region "A" contains very fine and rounded eutectic Si particles (Fig. 1d), termed globular-like eutectic. This region appears to be the first to grow from the nucleant. It appears that this microstructure zone is completely eutectic. This suggests that the liquid has undercooled to the coupled zone region on the phase diagram [19]. When a transition in morphology occurs at a certain position in the powder, primary Si interfaces begin to form. It appears that region "A" represents the growth of the microstructure during the recoalescence period of solidification and at the end of recalescence the elongated Si starts to form. Following the completion of elongated Si formation, eutectic forms. A sharp boundary delineating the regions between the growth during and post recalescence is clearly evident. Regions adjacent to microstructural transition line appear to have different eutectic length-scales as can be seen in the SEM image in Fig. 1(b, c and d). Finer eutectic Si particles correspond to zone "A"; whereas coarser eutectic Si particles refer to the other microstructure zones.

3.2. Quantification of zones in the microstructure

Volume fractions of zone "A" (f_{fine}) were measured as a function of powder size using image processing software (Image J). At least 10 images were examined to yield the value corresponding to each point (circles) inserted in Fig. 2a. An average value of each size range is considered for the present investigation. Fig. 2a shows that the fraction of the refined zone increases with decreasing powder size.

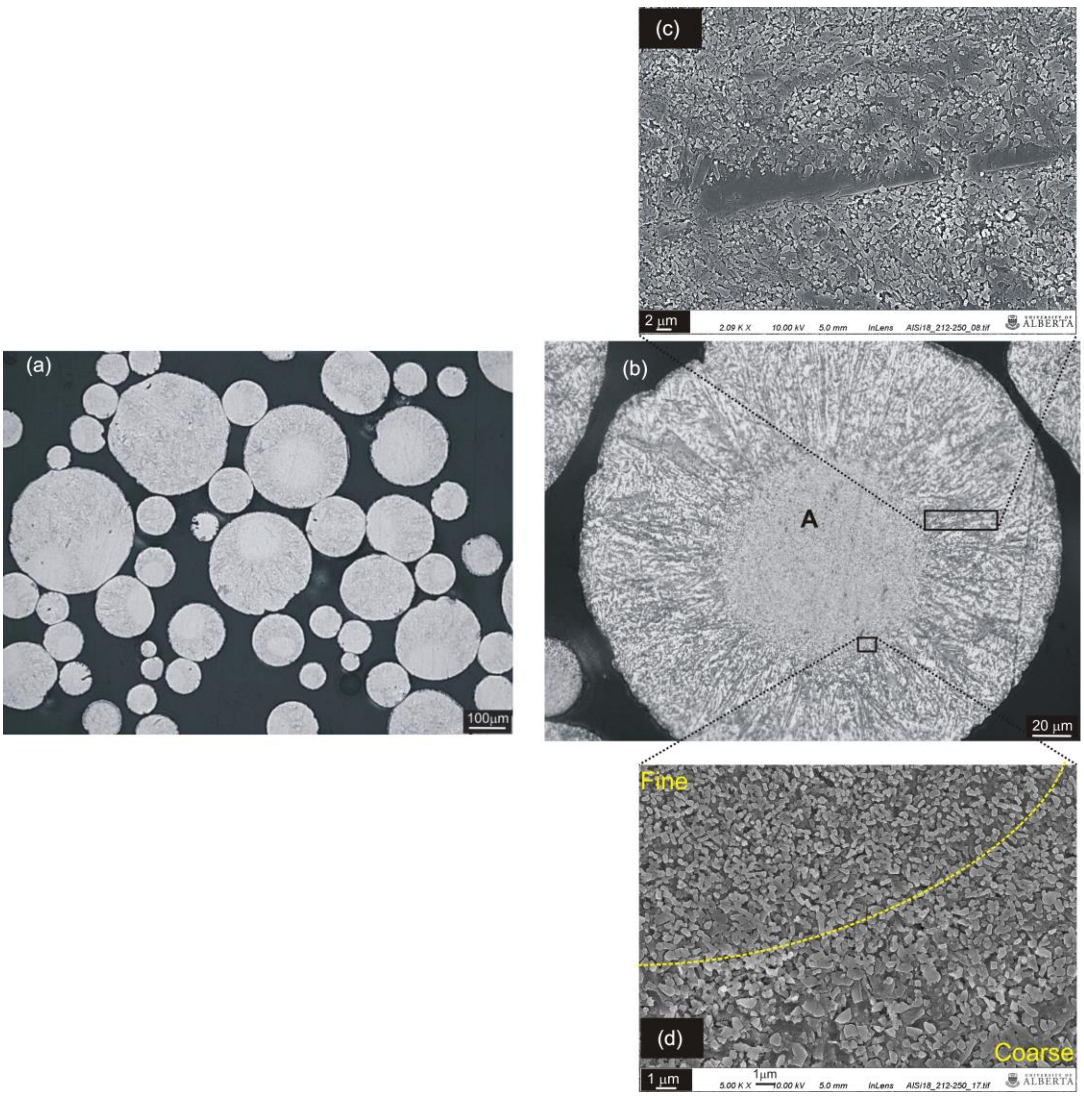

Fig. 1. (a) Representive optical image of the IA Al-18wt.%Si alloy powders and (b) cross-section optical and SEM images of an IA powder 212-250 µm in size showing both the formed two-zones and the eutectic Si particles within the fine and coarse zones adjacent to the microstructural transition. (c) and (d).

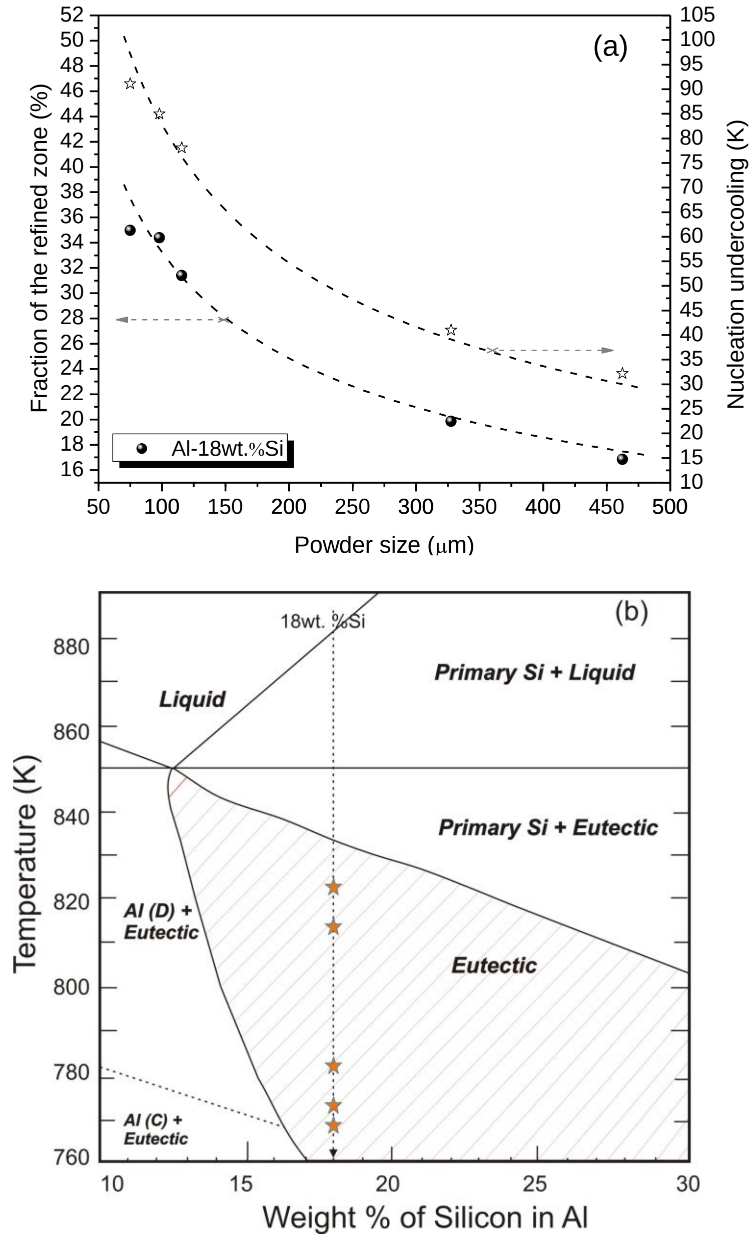

Fig. 2. (a) Zone A volume fraction and nucleation undercooling of the Al-18wt. %Si alloy as a function of the investigated powders sizes; and (b) the projection of ΔT values (stars symbols) in comparison with the predictions from literature considering the couple zone concept [19].

Considering the same powder sizes, the computed ΔT_N (Equation [6]) are also plotted in Fig. 2a (star symbols). As expected, the behavior of the nucleation undercooling parallels the evolution of the volume fractions [25,34]. The nucleation undercoolings of the primary eutectic zone are confined within the coupled zone region as outlined in the coupled zone diagram conceived for the Al-Si system in Fig. 2b. Therefore, the undercoolings are in very good agreement with previously calculated undercoolings associated with the eutectic microstructure region of the Al-18wt.%Si alloy. This explain the formation of this very refined eutectic zone promoted by high solidification velocity according to other previous investigation on this research topic [17-19].

The hypercooling limit concept has been recently applied in order to calculate the primary dendritic undercoolings (ΔT_p) of IA hypoeutectic Al-Cu powders. Bogno *et al.* [25] observed a good agreement between the experimentally estimated undercoolings using a coarsening model with those theoretically calculated using the hypercooling limit equation.

3.3 Morphologies of Si and their spacing

A typical spatial view of the microstructure of Al-18Si alloy powder can be seen in Fig. 3. Six positions are labeled starting from a position close to point of nucleation (#1) to the opposite diameter of the particle (#6). For this particle the point of nucleation was near or at the surface of the powder. Different regions in the powder show a clear variation in Si morphology. Each of the 6 positions (labelled #1, #2, #3, #4, #5 and #6) per powder cross section was examined and quite evident variations in the microstructure of the solidified powder are observed. While very fine microstructural features can be found near the nucleation site (positions #1 and #2 in Fig. 3), coarser Si particles are seen farther away from the nucleation site (#5 and #6). In this case of the IA powder 212-250 μm in size, globular morphology was observed for the three first positions closest to the nucleation site. As we move away from the point of nucleation, the morphology of Si becomes more fibrous and coarser.

The other two powder size ranges (106-125 μm and 425-500μm) also studied, showed similar observations. The presence of globular-like eutectic Si particles is more pronounced in smaller powders (106-125 μm) even for positions outside the primary eutectic zone while a high incidence of fibrous structures has been noted for the positions in the larger examined powders (425-500μm).

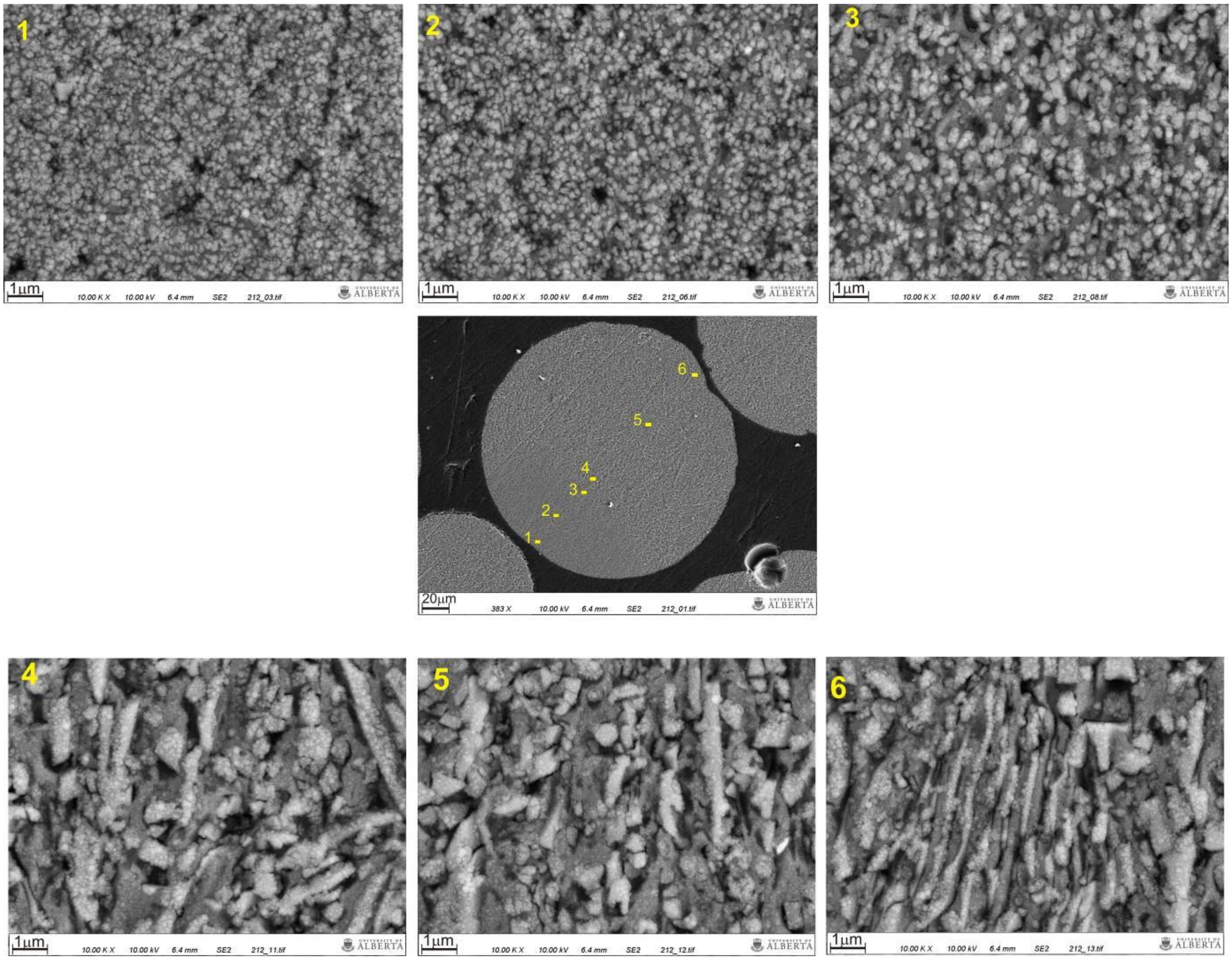

Fig. 3. Typical microstructure evolution of the IA powder 212-250 μm in size emphasizing the selected points and their corresponding SEM images (magnification of 10,000x) along the Al-18wt.%Si alloy powder diameter.

Interparticle spacing, λ, was measured for each powder as a function of the position from the nucleation point along the growth direction within the two zones. Fig. 4 shows a typical variation of the average λ values along with their standard deviations established for the powder of size 425-500μm. Linear dashed lines were inserted just to follow the experimental trends. Two different growth characteristics can be noted along the experimental evolution of λ. While the λ strongly increases for the positions inside the primary eutectic zone, a tendency of stability on the microstructure size can be seen if considered the last three points afar from the nucleation site. The shape of the Si morphology is also shown on Fig. 4.

Fig. 5a shows the variation of average interparticle spacing as a function of the normalized position on each investigated powder. Normalized position is represented by the distance from the nucleation site (denoted by 0%) and the particle surface furthest away (denoted by 100%). Also in Fig. 5 the boundary between the respective region "A" and the elongated Si surrounded by the coarser eutectic zone is indicated. Note that the boundary seems to occur generally about one third of the distance away from the nucleation site. As can be seen, the interparticle spacing increases with the relative position for all examined powder sizes ranges. The λ of larger powders is found to be greater than the λ of the finer ones for any evaluated position along the powder. Measurements carried out in positions adjacent to the morphological transition line, corresponding with both microstructure edges within the powder, show a significant difference in λ.

It can be seen in Fig. 5a that a strong variation in λ may occur when compared the measurements near the nucleation site with those near the surface of a certain powder. Considering these extreme positions (#1 and #6), the interparticle spacing increases about 5, 4 and 3 times for the powders of sizes 106-125 μm, 212-250 μm and 425-500 μm, respectively. Therefore, a wide range of cooling rates from the nucleation site to the powder surface seems to be associated with the smallest size powders.

3.4. Eutectic growth kinetics

Using the modified Jackson-Hunt (JH) analysis presented in the Equations [1] to [4] and from the values of λ measured in both microstructure zones of the Al-Si powders (see Fig. 5a), both the interface undercooling and the velocity of the eutectic can be computed and are presented in Fig. 5b and Fig. 5c, respectively. By comparing the scattered points in the graphs of Figs. 5a-c, as expected, for the three examined ranges of powder sizes, the solidification velocity and the growth undercooling decrease from the position #1 to the position #6 along the powders. In contrast, the interparticle spacing increases. This means that the evolutions of the kinetic parameters are reversely translated resulting in increase of the eutectic structure (interparticle spacing) for positions far from the nucleation site.

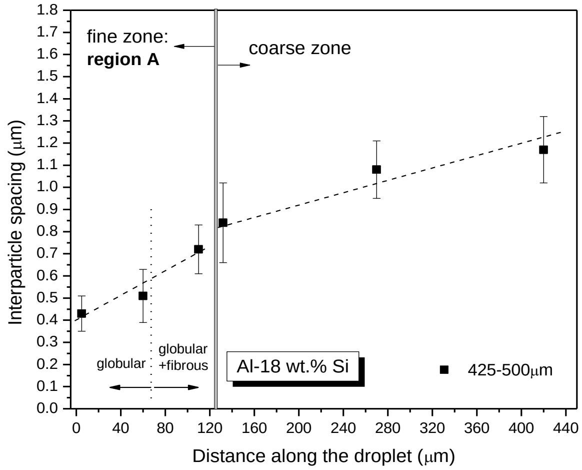

Fig. 4. Variation in range of the interparticle spacing as a function of the distance along the powder for the Al-18wt%Si of size 425-500µm generated by IA under He atmosphere.

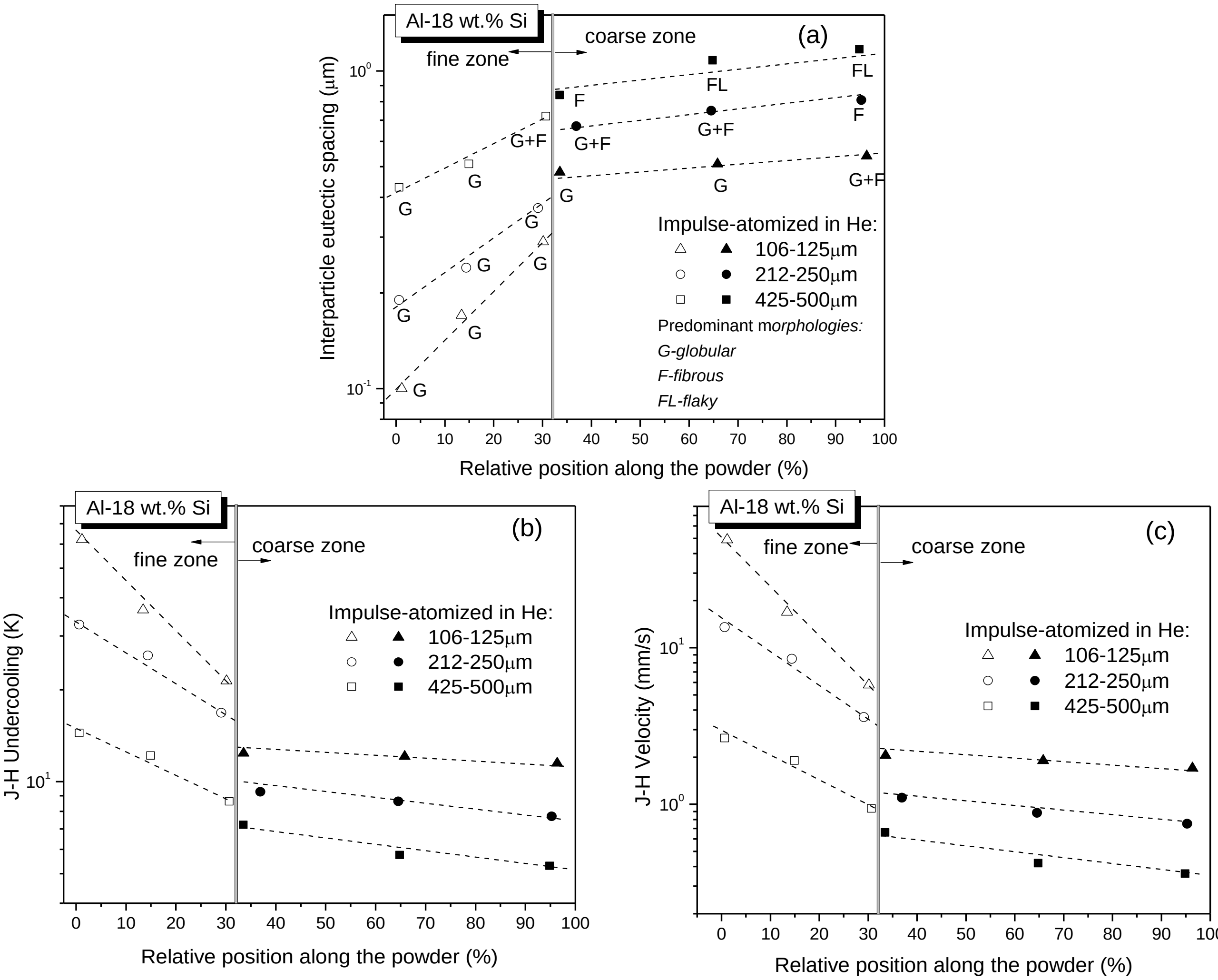

Fig. 5. (a) Average interparticle spacing, λ, (b) interface undercooling, ΔT, and (c) Interface velocity, V, as a function of the relative position along the Al-18wt.%Si alloy powder.

The maximum eutectic growth speed predicted by Pierantoni et al. [17] for laser-melted Al-18Si alloy tracks was ~62 mm/s, which is in reasonable agreement with the maximum of ~50 mm/s estimated in the present investigation for the smallest size powders.

Garcia et al [35] developed an analytical thermal analysis for the unidirectional solidification of metals in a casting. Fig. 6 presents a schematic of the adaptation of the method to a spherical particle. This analysis is used to describe the displacement of eutectic solidification front considering the one-dimensional spherical configuration, neglecting either convection in the melt or volume changes due to different densities of liquid and solid; and considering the absence of superheat in the liquid. It can be considered an approximatively unidirectional flow of heating within the powder along the diameter. This will be used to estimate the eutectic cooling rate.

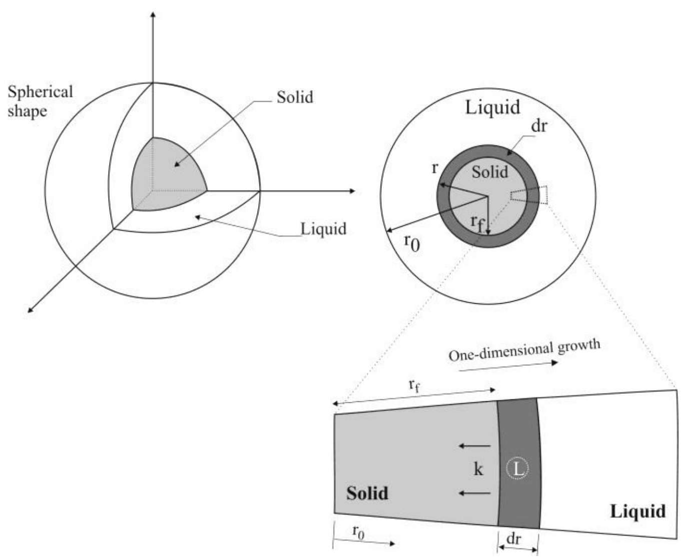

Fig. 6. Schematic representation of the thermal balance for radial geometries considering each side of the eutectic solidification front along the atomized powder. L is latent heat of fusion and k is the thermal conductivity. r_0 is the radius of sphere and r_f is the radius of the freezing eutectic front.

As described in the schematic of Fig. 6, an energy balance considering each side of the solidification front imposes:

$$k\left(\frac{dT}{dr}\right)_{r=rf} = Ld\left(\frac{dr_f}{dt}\right), \qquad [7]$$

where k is the thermal conductivity of the liquid, L is the latent heat of fusion and d is the density of the liquid. dr is an incremental solid layer as solidification advances; and r_f is the radius of the freezing eutectic front. The thermal energy per time in the right side of the Equation [7] must be equal to the energy transported by conduction (left side).

The left side term in the Equation [7] is the Fourier's law of heat conduction in radial coordinates, which is able to determine the rate of heat along radial direction. This term means the conductive heat flux within the alloy [36]. The Fourier's equation is able to represent a transient heat transfer process, assuming that the one-dimensional heat conduction within the solid is proportional to the temperature difference across the medium.

Based on the Eq. [7], it can be written:

$$k.\ G_E = L.d.\ V_E \qquad [8]$$

or

$$G_E = [(L.d)/k]\ .\ V_E \qquad [9]$$

or

$$G_E = C_1.\ V_E \qquad [10]$$

The eutectic cooling rate, CR, is given by:

$$CR = \left(\frac{dT}{dt}\right)_{r=rf} = \left(\frac{dT}{dr}\right)_{r=rf} \cdot \left(\frac{dr}{dt}\right)_r = G_E V_E \qquad [11]$$

By inserting Eq. [10] into Eq. [11], the cooling rate, CR, of the eutectic front will be given by an expression of the form:

$$CR = C_1 V_E^2 \quad or \quad CR = C_1 V_{JH}^2\ , \qquad [12]$$

where C_1 is the first term of the right side of Eq [9]: (L.d)/k, which is a constant value for a given alloy composition.

Previous data [3,37] devoted to the microstructural growth and kinetic parameters during directional solidification of the hypereutectic Al-18wt.%Si alloys under unsteady-state regime allowed to establish a linear function describing experimentally inferred cooling rate (CR) against the square of growth velocity (V^2), which was CR=1.6.10^7 (V^2). Both solidification thermal parameters have been determined based on the cooling curves recorded by thermocouples positioned along the length of the directionally solidified (DS) Al-18Si alloy casting. Both CR and V were determined around the eutectic temperature of the alloy.

According to the abovementioned Equations [9] and [12], the slope of the linear fitting CR x V^2 refers to the term (L.d)/k. Therefore, a good agreement is observed between the experimentally estimated C_1 values of 1.6 x 10^7 K.s.m^{-2} with that theoretically calculated of 1.5 x 10^7 K.s.m^{-2}. This can add support to the application of the Equation [12] in order to calculate the eutectic cooling rates from the position #1 to the position #6 along the Al-Si alloy powders.

Considering that CR is given by a constant (C_1) x V^2 [35] and substituting this expression into that of Jackson and Hunt [Equation 1], λ becomes directly proportional to -1/4, which is in agreement with the experimental growth law for λ variation in range as a function of cooling rate derived in the present study as shown in Fig. 7a. The estimated 9 points in the graph of Fig. 7a are associated with the positions #1, #2 and #3 of the powders with 106-125 μm, 212-250 μm and 425-500 μm in size. A wide range of cooling rates is indeed associated with the smallest size powders (triangle symbols), which is in accordance with the largest variation in range of the interparticle spacing within these powders as observed in Fig. 5a.

The modelling and characterization techniques employed in the present investigation allowed to determine G_E and V_E and relate those values to each Si morphology found on IA powders. These results were all combined on a eutectic Si morphology map as can be seen in Fig. 7b, showing 4 regions with distinct morphology, which are globular, globular+fibrous, fibrous and flaky. The cooling rate levels favoring each morphology incidence are shown in Fig. 7b.

Morphological information observed by several investigators [3,14,37-40] over a range of solidification velocities and thermal gradients are shown in Fig. 7b. Most of the inserted points from literature lay inside the regions proposed in the diagram. Toloui and Hellawell [39] affirmed that the transition from a flake to fibrous morphology is primarily dependent on growth rate and less clearly dependent on temperature gradient. However, it seems that the incidence of a certain morphology may depend on both thermal parameters. For instance, if one consider a V~0.9mm/s for higher G (17K/mm), start of globules can be seen, however, lower G (8K/mm) at the same V induces only the formation of fibers (see Fig. 7b). Similarly, a prevalence of globules is noted for V~2.0mm/s if a G of 37K/mm is assumed whereas a G of 9K/mm for the same V results in a mixture of globules and fibers.

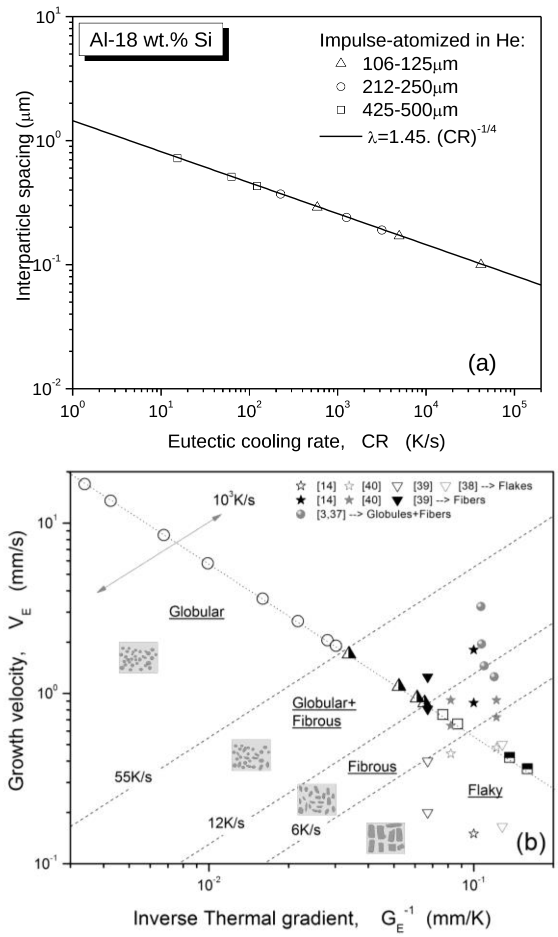

Fig. 7. (a) Interparticle spacing as a function of the eutectic cooling rate (CR) and (b) a diagram for the eutectic Si morphology based on IA results as well as other investigations.

3.5. Hardness vs. interparticle spacing related to different Si eutectic morphologies

The SEM microstructures in Fig. 8 are associated with very high strength based on the measured Vickers microhardnesses of 95HV, 115HV and 130HV for the regions very near the nucleation site in the Al-18wt.%Si powders of size 425-500 μm, 212-250 μm and 106-125 μm, respectively. For all the three examined microstructures, a major presence of very refined eutectic silicon globules can be noted.

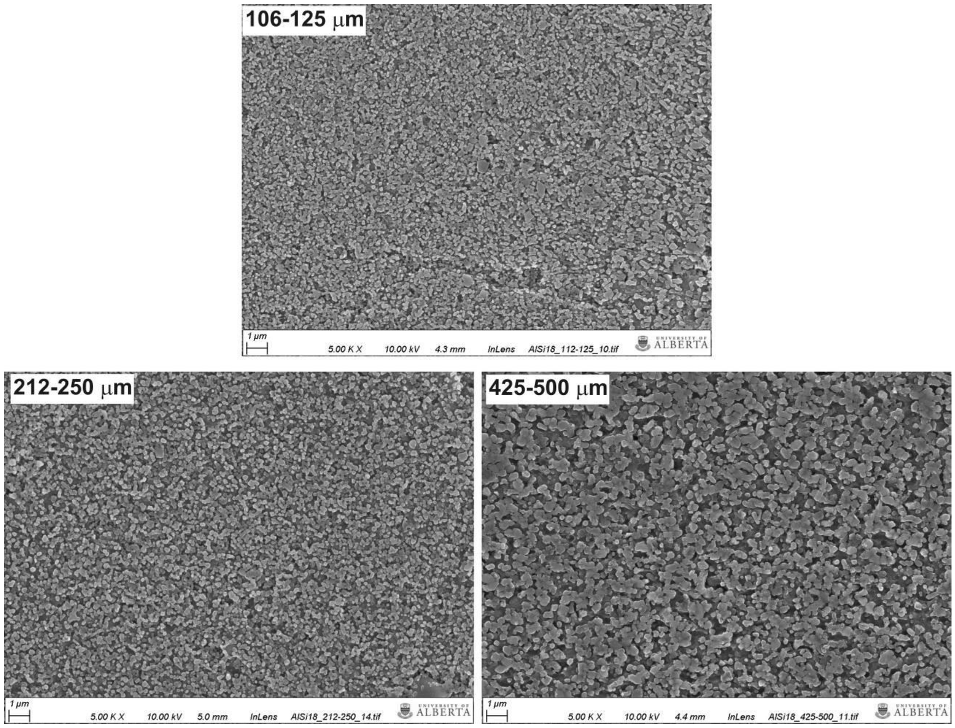

Fig. 8. Comparison of the most refined microstructures referring to the nucleation sites for the Al-18wt.%Si powders of sizes 106-125 μm, 212-250 μm and 425-500 μm generated by IA under helium atmosphere.

Islam et al. [41] have shown that globular-like particles associated with a fine eutectic mixture increase the mechanical strength. These particles can hind the movement of the dislocation lines inducing better mechanical behavior. On the other hand, considering microstructural arrays composed by columnar-like particles (see Fig. 3), the decrease in the tensile strength is expected because of the movement of dislocation lines, which can easily cross the lattice.

Indeed, the mentioned microhardness values are relatively higher than the values reported by Kang *et al.* [9], which examined SLM processed Al-18Si samples obtained at several laser powers. In this case, the microhardness decreases continually from 105 HV at 210 W to 80 HV at 120 W. These authors state that the nano silicon particles disappeared, being replaced by large separated Si grains, which is considered the prime factor leading to the low hardness value. The Vickers microhardness variations against the interparticle spacing are shown in Fig. 9a for the three investigated powders size ranges considering either globular-like or fibrous-like samples. Considering that most of the available studies on eutectic Al-Si have used either Bridgman type resistance heated furnaces [40] or water-cooled directional solidification setups [3,37] to produce directionally solidified samples and measure their microhardnesses, other compilations of results from literature were inserted in Fig. 9. Therefore, very broad ranges of cooling conditions and interparticle spacing considering results obtained by both directional solidification apparatus and impulse atomization could be examined.

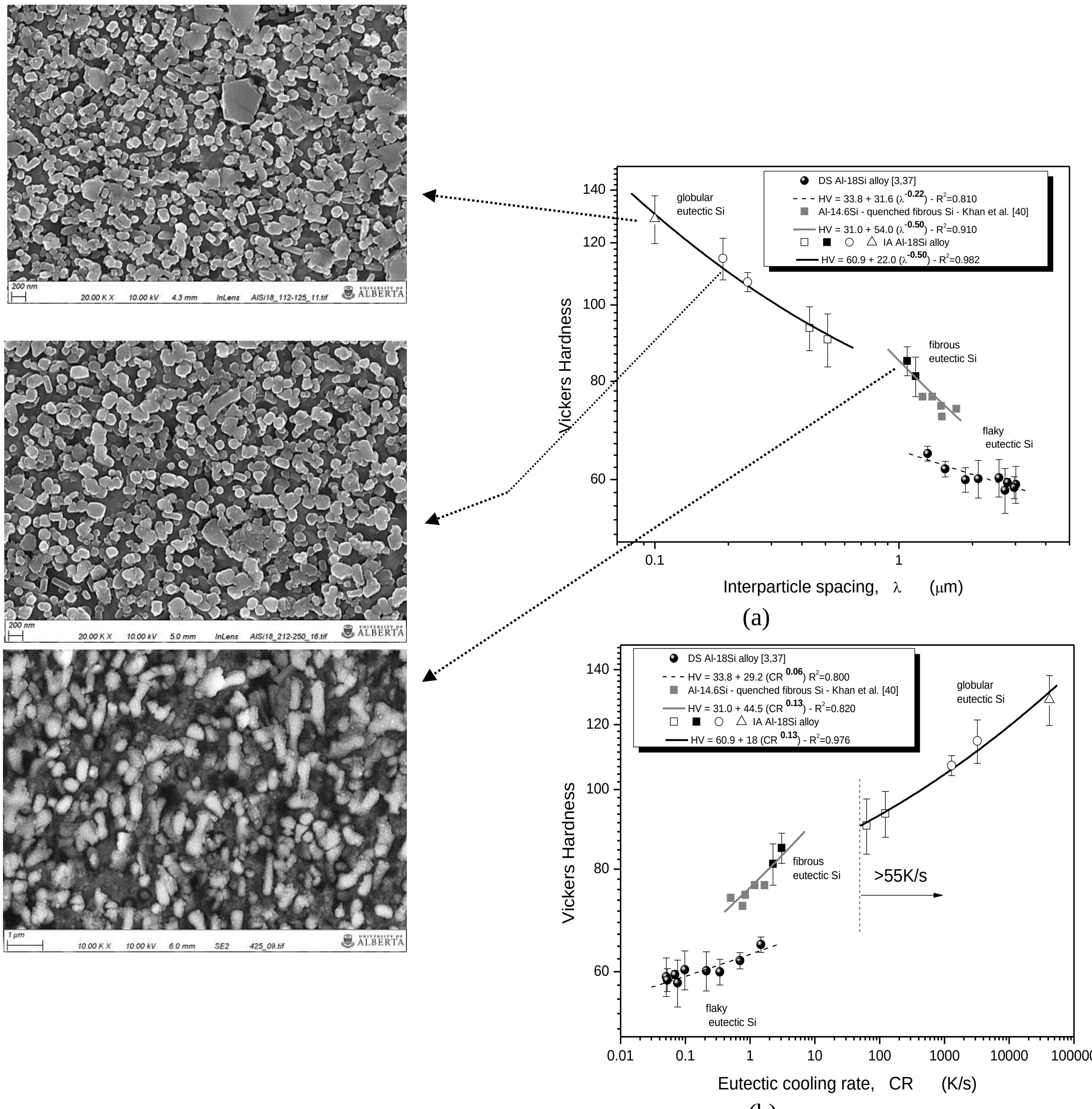

Fig. 9. Powder particle Vickers hardness (HV0.05 scale) as a function of (a) the interparticle spacing and as a function of (b) the eutectic cooling rate considering Si morphologies such as flakes, fibers and globules. R^2 is the coefficient of determination of a fitted curve.

It can be observed that the hardness is higher in globular Si samples as compared to fibrous and flaky ones. Flaky eutectic Si may lead to the lower hardness values. It is well known that the variations in hardness with both interparticle spacing (λ) and cooling rate (CR) can be given by [38]:

$$H=H_0+K\,(CR)^n\ , \qquad [13]$$

and

$$H=H_0+A\,(\lambda)^{-d}, \qquad [14]$$

where H_0 is the initial hardness , 'K' and 'A' are constants and 'n' and 'd' are constants depending on the silicon morphology. Based on the trendlines proposed in Fig. 9 for globular, fibrous and flaky silicon the values of d and n are -0.5/0.13, -0.5/0.13 and -0.22/0.06, respectively. The 'd' exponent of 0.22 for flaky Si calculated by Khan et al. [40] is in agreement with that proposed in Fig. 9(a) for the same morphology. The experimental exponent (-0.5) for the hardness-interparticle spacing relationship governing the globular silicon eutectic morphology was shown to be the same exponent as that adopted for the fibrous Si.

The growth of Si globules in the eutectic regions of the Al-18wt.% Si powders took place for relatively high cooling rates, i.e., it can be considered a morphological transition since the eutectic Si particles having round morphology prevailed for cooling rate (CR) higher than 55K/s (see Fig. 9(b)) or for solidification velocities higher than 1.8mm/s. According to Biswas *et al.* [15], globular morphology was found to prevail for as-lasered processed Al-Si eutectic samples under scan speed of 1.2 mm/s. Hosch *et al.* [14] reported a range of silicon growth mechanisms at several studied velocities (0.01– 2.0 mm/s) for the Al-13wt.%Si alloy, and the interval 0.1-0.95mm/s was related to the flake-to-fiber transition. These authors do no mention a changing in growth from fiber-to-globule, despite processing samples at 2.0mm/s. However, the conducted Bridgman-type experiments followed thermal gradients (G) of 7-14K/mm. Therefore, for a V of 2.0mm/s, a maximum cooling rate (CR) of 28K/s was achieved during eutectic solidification, since $CR=G.V$. This explain why globular morphology has not been developed during solidification generated by the Bridgman-type furnace, because the imposed cooling rate was at least 2 times lower than the critical value to the major growth of eutectic Si globules found in the present investigation.

4. Conclusions

The following major conclusions can be drawn from the present study:

1. The Al-18Si alloy powder microstructures radiating from the nucleation event consist of two zones of fine eutectic structure and coarse primary Si coupled with eutectic regions, being this change of microstructure features an effect of the time and position variations of the interface (eutectic) velocity. The primary eutectic zone developed around the nucleation point, probably during the recalescence stage, while an equilibrium microstructure filled up the rest of the powder volume and occurs during the remaining stage of solidification, past recalescence. The primary nucleation undercoolings determined for various powder sizes lay inside the eutectic coupled zone region as previewed by the coupled zone concept for the Al-Si system.

2. From interparticle eutectic spacing values, the evolutions of either the eutectic cooling rate or the velocity were calculated. These solidification thermal parameters decrease as solidification proceeds from the nucleation event to the surface of the powder. These evolutions were reversely translated resulting in increase of the interparticle spacing for distinct positions from the nucleation point. The interparticle spacing increases about 5, 4 and 3 times for the powders of sizes 106-125 μm, 212-250 μm and 425-500 μm, respectively.

3. It was demonstrated the prevalence of a substantial number of Si globules with positions inside the fine eutectic zone because of the higher cooling rates. Overall, for positions outside the primary eutectic zone a high incidence of fibrous structures was noted, especially for the largest examined size powder. There is clear indication that the coalescence of globules gives rise to the formation of fibers (or mixture of fiber and globules). The cooling rates and solidification velocities during growth of the atomized powders are shown to affect the morphology of the Si particles, from globular > mixture of globular and fibrous> fibrous> mixture of fibrous and flaky.

4. A more effective inhibition of dislocation lines displacement during load probably induced higher microhardnesses related to the fine globular silicon eutectic morphology. It is shown that the prevalence of globular Si eutectic morphology in impulse atomized Al-18Si alloy powders is possible for CR > 55 K/s.

Acknowledgements

The authors are grateful to FAPESP (São Paulo Research Foundation, Brazil: grants 2015/11863-5 and 2016/10596-6) for their financial support. Support from the Natural Science and Engineering Research Council is also gratefully acknowledged.

References

[1] J.W. Bray: ASM Metals Handbook. 1976, vol. 2, 10th ed., ASM Intl..
[2] V.S. Zolotorevsky, N.A. Belov, M.V. Glazoff, Casting aluminum alloys, 2007, vol. 12, Elsevier.
[3] R.V. Reyes, T.S. Bello, R. Kakitani, T.A. Costa, A. Garcia, N. Cheung, J.E. Spinelli: Mater. Sci. Eng. A., 2017, vol. 685, pp. 235-243.
[4] M. Tebib, F. Ajersch, A.M. Samuel, X.-G. Chen: Metall. Mater. Trans. A., 2013, vol. 44 , pp. 4282-4295.
[5] L. Lasa, JM. Rodriguez-Ibabe: Mater. Sci. Eng. A., 2003, vol. 363, pp. 193-202.
[6] K. Matsuura, M. Kudoh, H. Kinoshita, H. Takahashi: Mater. Chem. Phys., 2003, vol. 81, pp. 393-395.
[7] Z. Kamberovic, E. Romhanji, M. Filipovic, M. Korac: Metallurgy, J. Metall., 2009, vol. 15, pp. 189-200.
[8] W.S. Miller, L. Zhuang, J. Bottema, A. Wittebrood, P. De Smet, A. Vieregge: Mater. Sci. Eng. A, 2000, vol 280, pp. 37-49.
[9] N. Kang, P. Coddet, H. Liao, T. Baur, C. Coddet: Appl. Surf. Sci., 2016, vol. 378, pp. 142-149.
[10] E.O. Olakanmi: J. Mater. Process. Tech., 2013, vol. 213, pp. 1387-1405.
[11] N. Kang, P. Coddet, H. Liao, C. Coddet: J. Alloy Compd., 2016, vol. 662, pp. 259-262.
[12] Y.E. Kalay, L.S. Chumbley, I.E. Anderson, R.E. Napolitano: Metall Mater Trans A, 2007, vol. 38, pp. 1452-1457.
[13] W.J. Boettinger, L. Bendersky, J. G. Early: Metall Mater Trans A, 1986, vol. 17, pp. 781-790.
[14] T. Hosch, L. G. England and R. E. Napolitano, J Mater Sci, 2009, v. 44, pp. 4892–4899.
[15] A. Biswas, B.L. Mordike, I. Manna and J.D. Majumdar: Lasers Eng., 2008, vol. 18, pp. 95-105.
[16] V.C. Srivastava, R.K. Mandal, S.N. Ojha: Mater. Sci. Eng. A, 2001, vol. 304-306, pp. 555-558.
[17] M. Pierantoni, M. Gremaud, P. Magnin, D. Stoll, W. Kurz: Acta Metall. Mater., 1992, vol. 40, pp. 1637-1644.
[18] S.P. Nikanorov, M.P. Volkov, V.N. Gurin, Yu.A. Burenkov, L.I. Derkachenko, B.K. Kardashev, L.L. Regel, W.R. Wilcox: Mater. Sci. Eng. A, 2005, vol. 390, pp. 63-69.
[19] R. Trivedi, F. Jin, I.E. Anderson: Acta Mater., 2003, vol. 51, pp. 289-300.
[20] A. M. Mullis, L. Farrell, R. F. Cochrane, and N. J. Adkins: Metall. Mater. Trans. B, 2013, vol. 44, pp. 992-999.
[21] J. D. Roehling, D. R. Coughlin, J. W. Gibbs, J. K. Baldwin, J. C.E. Mertens, G. H. Campbell, A. J. Clarke, J. T. McKeown: Acta Mater., 2017, vol. 131, pp. 22-30

[22] H. Henein, V. Buchoud, R. Schmidt, C. Watt, D. Malakov, C-A. Gandin, G. Lesoult, V. Uhlenwinkel: Can. Metall. Quart., 2010, vol. 49, pp. 275-292.

[23] J.B. Wiskel, K. Navel, H. Henein, E. Maire: Can. Metall. Quart., 2002, vol. 41, pp. 193-204.

[24] J.B. Wiskel, H. Henein, E. Maire: Can. Metall. Quart., 2002, vol. 41, pp. 97-110.

[25] A.-A. Bogno, P. Delshad Khatibi, H. Henein, Ch.-A. Gandin: Metall. Mater. Trans. A, 2016, vol. 47, pp. 4606-4615.

[26] M Gunduz, E Çadirli: Mater Sci Eng A, 2002, vol. 327, pp. 167-185.

[27] M. Gündüz, H. Kaya, E. Çadırlı, A. Özmen: Mater Sci Eng A, 2004, vol. 369, pp. 215-229.

[28] K.A. Jackson, J.D. Hunt: Lamellar and rod eutectic growth, T Metall Soc AIME, 1966, vol. 236, pp. 1129-1142.

[29] P. Magnin, J.T. Mason, R. Trivedi: Acta Metall. Mater., 1991, vol. 39, pp. 469-480.

[30] T. Magnusson, L. Arnberg: Metall. Mater. Trans. A, 2001, vol. 32, pp. 2605-2613.

[31] R. Brandt, G. Neuer: Int. J. Thermophys, 2007, vol. 28, pp. 1429-1446.

[32] B.M. Angadi, R. Hiremath, A. Chennakesava Reddy, Last S. A. Kori: J Mec. Eng. Res Technol., 2014, vol. 2, pp. 536-544.

[33] Z. Zhang, X. Bian, Y. Wang, X. Liu: T Nonferr Metal Soc, 2001, vol. 11, pp. 374-377.

[34] J.W. Martin, R.D. Doherty, B. Cantor: Stability of microstructure in metallic systems, 1997, Cambridge University Press, 426p.

[35] A. Garcia, T.W. Clyne, M. Prates: Metall. Trans. B, 1979, vol. 10, pp. 85-92.

[36] M. E. Glicksman: Principles of Solidification. Chapter 3: Thermal Concepts in Solidification, 2011, Springer New York., pp. 53-68.

[37] R.V. Reyes, R. Kakitani, T.A. Costa, J.E. Spinelli, N. Cheung, A.: Phil. Mag. Lett., 2016, vol. 96, pp. 228-237.

[38] H. Kaya, E. Çadirli, M. Gündüz and A. Ulgen: J. Mater. Eng. Perform., 2003, vol. 12, pp. 544-551.

[39] B. Toloui, A. Hellawell: Acta Metall., 1976, vol. 24, pp. 565-573.

[40] S. Khan, A. Ourdjini, Q. S. Hamed, M. A. Alam Najafabadi, R. Elliott: J. Mater. Sci., 1993, vol. 28, pp. 5957-5962.

[41] R.A. Islam, Y.C. Chan, W. Jillek, S. Islam: Microelectron. J., 2006, vol. 37, pp. 705-713.

Table heading

Table 1. Summary of data used for the investigated Al-Si alloy [12,29,30-33].

Figure captions

Fig. 1. (a) Representive optical image of the IA Al-18wt.%Si alloy powders and (b) cross-section optical and SEM images of an IA powder 212-250 μm in size showing both the formed two-zones and the eutectic Si particles within the fine and coarse zones adjacent to the microstructural transition. (c) and (d).

Fig. 2. (a) Zone A volume fraction and nucleation undercooling of the Al-18wt. %Si alloy as a function of the investigated powders sizes; and (b) the projection of ΔT values (stars symbols) in comparison with the predictions from literature considering the couple zone concept [19].

Fig. 3. Typical microstructure evolution of the IA powder 212-250 μm in size emphasizing the selected points and their corresponding SEM images (magnification of 10,000x) along the Al-18wt.%Si alloy powder diameter.

Fig. 4. Variation in range of the interparticle spacing as a function of the distance along the powder for the Al-18wt%Si of size 425-500μm generated by IA under He atmosphere.

Fig. 5. (a) Average interparticle spacing, λ, (b) interface undercooling, ΔT, and (c) Interface velocity, V, as a function of the relative position along the Al-18wt.%Si alloy powder.

Fig. 6. Schematic representation of the thermal balance for radial geometries considering each side of the eutectic solidification front along the atomized powder. L is latent heat of fusion and k is the thermal conductivity. r_0 is the radius of sphere and r_f is the radius of the freezing eutectic front.

Fig. 7. (a) Interparticle spacing as a function of the eutectic cooling rate (CR) and (b) a diagram for the eutectic Si morphology based on IA results as well as other investigations.

Fig. 8. Comparison of the most refined microstructures referring to the nucleation sites for the Al-18wt.%Si powders of sizes 106-125 μm, 212-250 μm and 425-500 μm generated by IA under helium atmosphere.

Fig. 9. Powder particle Vickers hardness (HV0.05 scale) as a function of (a) the interparticle spacing and as a function of (b) the eutectic cooling rate considering Si morphologies such as flakes, fibers and globules. R^2 is the coefficient of determination of a fitted curve.